



Deposited via The University of Leeds.

White Rose Research Online URL for this paper:

<https://eprints.whiterose.ac.uk/id/eprint/222075/>

Version: Accepted Version

---

**Article:**

de Pablo, J.G., Lindley, M., Hiramatsu, K. et al. (2023) Label-free live microalgal starch screening via Raman flow cytometry. *Algal Research*, 70. 102993. ISSN: 2211-9264

<https://doi.org/10.1016/j.algal.2023.102993>

---

© 2023 Elsevier B.V. All rights reserved. This is an author produced version of an article published in *Algal Research* made available under the CC-BY-NC-ND 4.0 license (<http://creativecommons.org/licenses/by-nc-nd/4.0>) in accordance with the publisher's self-archiving policy.

**Reuse**

This article is distributed under the terms of the Creative Commons Attribution-NonCommercial-NoDerivs (CC BY-NC-ND) licence. This licence only allows you to download this work and share it with others as long as you credit the authors, but you can't change the article in any way or use it commercially. More information and the full terms of the licence here: <https://creativecommons.org/licenses/>

**Takedown**

If you consider content in White Rose Research Online to be in breach of UK law, please notify us by emailing [eprints@whiterose.ac.uk](mailto:eprints@whiterose.ac.uk) including the URL of the record and the reason for the withdrawal request.

# Label-free live microalgal starch screening via Raman flow cytometry

Julia Gala de Pablo<sup>1,2</sup>, Matthew Lindley<sup>1</sup>, Kotaro Hiramatsu<sup>1</sup>, Akihiro Isozaki<sup>1</sup> and Keisuke Goda<sup>1,3,4\*</sup>

<sup>1</sup> Department of Chemistry, The University of Tokyo, Tokyo, Japan

<sup>2</sup> School of Biomedical Sciences, University of Leeds, Leeds, United Kingdom

<sup>3</sup> Department of Bioengineering, University of California, Los Angeles, CA, United States

<sup>4</sup> Institute of Technological Sciences, Wuhan University, Wuhan, China

## ABSTRACT

Microalgal carbon fixation attracts much attention as an environmentally friendly source of biomaterials. In this context, microalgal starch plays an important role because it can be converted to bioethanol and bioplastics. However, optimizing culturing conditions and generating strains with higher starch productivity is still a challenge primarily due to the lack of methods for screening starch content at a single-cell level; established starch quantification methods are time-consuming, reagent-consuming, and destructive. Here we report a high-throughput, starch-screening method based on Raman flow cytometry by measuring molecular vibrations that can be used in suspended cells in their growth medium. Our method obtains the full fingerprint spectrum of starch, providing increased specificity when compared to narrow-band Raman spectroscopy methods. Specifically, we demonstrated label-free, single-cell-resolved screening of intracellular starch in cells of microalgal species *Chromochloris zofingiensis* that overcame the above problems and achieved >30-100 times higher event rate than previous methods, which enabled the acquisition of >20 times more cells in a fraction of the time. We screened the single-cell starch contents of about 28,000 *C. zofingiensis* cells cultured under 14 different conditions (~2,000 cells per condition) to adjust culture conditions for starch accumulation. Comparing the data against Lugol staining and bulk-sample enzymatic starch quantification showed the potential of Raman flow cytometry for mean starch quantification. Raman flow cytometry showed higher sensitivity than Lugol staining and linear dependence with the mean per-cell starch ratio

obtained from enzymatic starch quantification. Raman flow cytometry enables single-cell label-free metabolite quantification and paves the way to accurate, cost-effective optimization of culturing conditions, with future applications in the screening of starch hyper-producing microalgae following mutagenesis or from environmental samples.

## **KEYWORDS**

Starch, flow cytometry, single-cell, live-cell screening, Raman, label-free

## **1. INTRODUCTION**

Microalgal carbon fixation and production of biomaterials have gained importance in the last decades. Its high carbon fixation capacity, fast growth, and simple growth requirements make it a promising countermeasure against global warming and famine [1]. In this context, starch, an abundant and biodegradable polysaccharide [2], plays an important role because it is accumulated in microalgae and can be converted to bioethanol and bioplastics. Among various sources of starch such as barley, wheat, corn, and rice, microalgal starch attracts much attention because it is solely composed of valuable small granules (~1  $\mu\text{m}$ ) [3,4] with different physicochemical properties than big granules due to their increased surface-to-volume ratio [5]. Small starch granules have applications in the food, paper, cosmetic, photographic, and textile industries, but are costly to produce and isolate from higher-order plants [6]. Another important advantage of using microalgae is that their growth does not require arable land [7], enabling the reuse of industrial wastewater as a culture medium. Achieving the economical sustainability of microalgal starch production is the key to enabling widespread industrial production [1]. To this end, microalgal culture conditions should be optimized for efficient starch accumulation.

To enhance the efficiency of microalgal starch production, a high-throughput and low-cost method for starch screening with single-cell resolution would be valuable, but no existing method meets all the requirements. Currently, microalgal starch screening is performed enzymatically, where microalgal biomass is disrupted and starch is hydrolyzed to glucose followed by colorimetric quantification [8–10]. Unfortunately, those methods are costly, reagent-demanding, destructive, and time-consuming and do not provide single-cell resolution [11]. In addition, a large number of cells (usually >500 million cells) are needed to obtain enough dry mass for quantification using the enzymatic methods (typically ~10 mg),

increasing the necessary culture sizes for optimization experiments (~50 mL). Alternatively, iodine staining, commonly referred to as Lugol staining, allows for imaging and colorimetric quantification of starch, but has a very limited quantifiable range [12] and is not applicable to live cells, impeding further culture after the measurement. Consequently, the unavailability of sensitive, fast, and convenient single-cell starch screening methods hinders obtaining highly productive strains and optimizing culturing conditions.

To overcome the above issues, Raman spectroscopy has been proposed as a promising technique for starch screening. Raman spectroscopy is a label-free non-destructive analytical technique that probes vibrational signatures of molecules by detecting molecular inelastic scattering [13]. It has been used to obtain rich structural information about intracellular molecules such as proteins, nucleic acids, and metabolites including starch [14–16]. For example, Ji *et al.* showed the potential of Raman spectroscopy for single-cell starch quantitative analysis by showing a linear correlation between the 60-cell average intensity of the 478  $\text{cm}^{-1}$  Raman band and bulk starch content in *Chlamydomonas reinhardtii* cells [11]. In further work by He *et al.* they showed that single-cell Raman spectroscopy could be used to quantify starch, proteins, and triacylglycerides [17]. Despite these advantages, spontaneous Raman scattering is inherently weak, limiting its cell analysis event rate [18] to typically <1 event per second (eps), where an event is defined as any particle, cell, cell cluster, or cell debris that triggers signal acquisition. For example, He *et al.* only measured 20 cells per culture, with 2-second acquisitions per cell, and required cell bleaching before Raman signal acquisitions [17]. Subsequently, the number of cells that can be interrogated is typically limited to less than a hundred, which hampers statistical analysis of cell ensembles.

In this article, we report high-throughput Raman flow cytometry [19] of microalgal starch content in *Chromochloris zofingiensis* cells using a Fourier-transform coherent anti-Stokes Raman scattering (FT-CARS) flow cytometer at an event rate of ~30-100 eps, which is >30-100 times higher than that of previously reported methods. As we previously demonstrated [20,21], our Raman flow cytometer enables rapid (24,000 spectra/s) acquisition of broadband (200 – 1,600  $\text{cm}^{-1}$ ) Raman spectra of cells flowing in a microfluidic chip [21], which makes it an ideal tool for rapid starch screening in microalgal cells. Specifically, we performed label-free flow cytometry of live *C. zofingiensis* cells cultured under different conditions to maximize their starch production. We studied the starch accumulation dependence on the glucose concentration and incubation time by analyzing more than 2,000 cells for each condition, >30 times more than previous reports

[11]. Furthermore, we compared our high-throughput Raman flow cytometry with standard starch screening techniques, namely Lugol staining and enzymatic quantification.

## 2. MATERIALS AND METHODS

**Microfluidic device.** The microfluidic device used was a borosilicate-silicon-borosilicate device as described in the reports by Hiramatsu *et al.* [20] and Sakuma *et al.* [22]. Briefly, the fabrication process combined glass sandblasting, silicon deep reactive ion etching, and anodic bonding, obtaining a  $200 \times 200 \mu\text{m}^2$  channel. A piezoelectric transducer (PZT) was adhered to the microfluidic device using cyanoacrylate adhesive for three-dimensional acoustic cell focusing. The application of a 60-V<sub>pp</sub> voltage at 3.66 MHz to the PZT resulted in the generation of acoustic standing waves that focused the cells to the middle of the channel. The cells were injected into the channel using a syringe pump at a flow rate of 50  $\mu\text{L}/\text{min}$ , resulting in a measured cell flow speed at the center of the channel of  $4.89 \pm 0.09 \text{ cm/s}$ .

**Optical setup.** The optical setup was based on the one described in the report by Hiramatsu *et al.* [20], using a pulsed Ti:Sapphire femtosecond mode-locked laser with a center wavelength of 780 nm, pulse FWHM of 80 nm, and a repetition rate of 80 MHz (Coherent, Vitara-T-HP) (Figure 1). To realize the transform-limited pulse at the sample position, the dispersion was compensated by combining chirp mirrors (Thorlabs, DCMP175) with a pulse shaping setup, consisting of a 4f system with a dispersive prism (Thorlabs, PS859), a cylindrical concave mirror (Thorlabs, CCM254-400-P01), and a spatial light modulator (SLM; Santec, SLM200), controlled by an in-house genetic algorithm optimizer. The optimization of the pattern on the SLM was performed via genetic algorithms using the water non-resonant background signal obtained around the zero pump-probe time delay as described in the report by Lindley *et al.* [23]. Orthogonally polarized pulse pairs with varying intra-pair optical delay were generated using a Michelson interferometer with a resonant scanner (Cambridge Technology, CRS 12 kHz), which generates a maximum optical path-length difference of 0.5 mm ( $18 \text{ cm}^{-1}$  spectral resolution) at an acquisition rate of 24,000 spectra/s. The delay for each pulse pair was tracked by monitoring interferograms of a co-propagating continuous wave (CW) laser (1064 nm). Before the sample, a long-pass filter (Thorlabs, FELH0750) removed the blue edge of the pulses. A pair of 50x objectives (Olympus, LCPLANN50X0.65IR) focused and collected the pulses. After interaction with the sample, the pump light was removed with a half-wave plate and polarizing beam splitter (Thorlabs, PBS252). The forward scattered anti-Stokes light was filtered with a short-pass filter (Thorlabs,

FESH0750) and detected by an avalanche photodiode (Thorlabs, APD120A/M). Forward scattering (FSC) of the flowing cell detected at an upstream position of the FT-CARS interrogation position using a 635-nm CW laser (Thorlabs, CPS635) was used for triggering FT-CARS detection. The FSC component reflected by the polarizing beam splitter was focused onto a spatial mask before the detector, using its rising edge as a trigger. For cytometry experiments, the laser power used ranged between 175 and 220 mW measured below the focusing objective and was measured prior to every experiment. The laser power after the focusing objective was ~70% of the reported values. The starch signal showed a cubic dependence with the laser power below the objectives (see Figures S1a and S1b). The maximum laser power available was used to maximize the signal to noise ratio.

**Spectrum data analysis.** Spectra were recorded along the line of flow, with ~30 spectra/event, and event rates between 30-100 eps. For each spectrum, the information of four channels of the digitizer was saved: the FT-CARS signal, the FSC signal used for triggering, the clock signal used for controlling the movement of the resonant scanner, and the co-propagating CW signal to calculate the optical delay between the two pulses at any given time. Spectral analysis was processed in Matlab (functions indicated in *italics*). The time-domain signal was chopped into individual spectra by using the clock signal. The phase of the 1064 nm CW interferogram was unwrapped to obtain the optical delay. The time-domain CARS data were interpolated using the optical delay data and Fourier transformed (*fft*) using a Hann window (*hann*) to obtain the spectra. The ~18 cm<sup>-1</sup> resolution spectrum was linearly interpolated (*interp1*) to 1 cm<sup>-1</sup> for convenience. Events that showed a sudden drop or increase of intensity in the time-domain CARS signal appeared as an exponentially decaying intensity in the frequency domain, showing very high intensity for low wavenumbers. These saturated events were filtered by comparing the intensity at 210 cm<sup>-1</sup> with the intensity at 1200 cm<sup>-1</sup>. The spectral intensity at ~35 cm<sup>-1</sup> attributed to four-wave mixing contributions in our time-domain spectrometer – caused by changes in the signal baseline – was used to identify the cell-containing spectra, perform cell averaging, and remove events that contained more than one cell. The Raman intensity reported corresponds to the integrated starch peak, calculated by summing the intensity of the peak with a width of ± 50cm<sup>-1</sup>. For starch quantification, the average intensity at a featureless wavenumber (690 cm<sup>-1</sup>) for each sample was used to subtract the average noise from the Raman intensity at the 478 cm<sup>-1</sup> peak. Due to variations of the instrument between days, the frequency of the strongest starch spectral peak varied in a range between 472-478 cm<sup>-1</sup>. The position of the peak maximum for each experiment was used for further analysis.

**Flow cytometry measurement.** Figure 1 shows an image of the acquisition area in the microfluidic device with the relative positions of the CW and the Ti:Sapphire femtosecond laser spots. In each acquisition, ~30 Raman spectra were taken along a line across a single cell (see Figure S1c). Each set of spectra was acquired every 1.26 ms, corresponding to the acquisition rate of ~800 eps. In practice, the cell flow was the bottleneck for the system event rate, usually resulting in event rates of 30-100 eps.

**Cell culturing.** *Chromochloris zofingiensis*, previously known as *Chlorella zofingiensis* or *Muriella zofingiensis* [24], cells were cultured as follows. The NIES 2175 strain was purchased from the National Institute of Environmental Studies (Japan). NIES 2175 cells were cultured in modified acetate media (mAc) prepared as AF6 media with 0.4 g/L glucose, 0.4 g/L yeast extract, 0.4 g/L tryptone, and 0.4 g/L sodium acetate. Cells were cultured with 120  $\mu\text{mol}/\text{m}^2\text{s}$  photon flux under 12h/12h light/dark cycles at 29-26°C. For enzymatic quantification, cells were cultured under the aforementioned conditions, but in 8h/16h light/dark cycles. For all experiments, saturated culture cells were counted and seeded in flasks or well plates and grown without agitation or CO<sub>2</sub> bubbling. Unless stated otherwise, 10<sup>5</sup> cells/mL were seeded in either low-glucose mAc (0.4 g/L glucose) or high-glucose mAc medium. Following cell culture, the cells could reach densities above 1×10<sup>7</sup> cells/mL. For Raman flow cytometry, the cell concentration was adjusted to 0.5-1×10<sup>6</sup> cells/mL and measured in mAc medium.

**Impedance flow cytometry.** Cell concentrations and sizes were measured using a commercial impedance flow cytometer (Sysmex Corporation, CDA-1000). Cells were suspended in a commercial buffer provided by Sysmex and analyzed for size distribution and cell concentration. To ensure the size accuracy of the instrument, a suspension of 6  $\mu\text{m}$  polystyrene beads suspension was used (data not shown).

**Lugol staining.** Cells were fixed with glutaraldehyde 2.5% for 10 min, washed, and stored in DPBS at 4°C. Lugol solution 5% I/10% KI was added to the cell suspension to a final concentration of 2%/4%. The mixture was incubated for 10 min and imaged with a 40× objective in a color microscope. For Lugol quantification, ImageJ was used to identify single-cell regions of interest and calculate the per-cell average intensity in the grey-intensity images from the color microscope. Images containing >480 cells per condition were analyzed. The background intensity was measured in >20 single background points for each of the conditions. Darker cell coloration and thus lower cell intensity values indicated the presence of starch.

**Cell viability.** For cell viability analysis, cells were incubated for 44-48 h following exposure to the laser. 4',6-diamidino-2-phenylindole (DAPI) was used as an exclusion dye by adding it to the cell suspension at a

final concentration of 0.2 µg/mL. Cells were incubated with DAPI in the dark and imaged using a fluorescent microscope (Nikon, Eclipse Ti) with a DAPI filter set. Nuclei DAPI staining indicated membrane permeability and was used to identify dead cells.

**Imaging and sizing of microalgal starch granules.** For starch granule imaging, cells were disrupted by autoclaving for 1 h at 135°C. Following autoclaving, both free and membrane-bound starch granules were imaged and sized. ImageJ was used for granule sizing. It should be noted that high temperatures can lead to granule swelling, and thus the granule sizes reported values are likely overestimated.

**Enzymatic quantification.** For enzymatic starch quantification, cell samples were seeded in T25 flasks covering a range of cell and glucose concentrations. Day 4 cells were measured with Raman flow cytometry. Aliquots from these samples were ethanol fixed and stored at 4°C prior to quantification. Following cell concentration measurement, each cell suspension was dried at 75°C until its mass was constant across periodic measurements. We then measured the sample dry mass and calculated biomass. Those cell samples with enough mass for starch quantification were disrupted in a mortar and analyzed following the “rapid total starch method” protocol from the Megazyme Total starch quantification assay kit (Megazyme, Neogen) commonly used in the literature [25], with UV-Vis values used to determine starch content.

### 3. RESULTS

#### 3.1 Characterization of starch accumulation

To confirm the detection of starch in microalgal cells, a wheat starch standard was compared to the signal of microalgal cells grown in high-glucose medium (Figure 2a). The spectra show an identical profile, indicating that intracellular starch is detected in the cell measurements. The positions of the main bands were in agreement with reported Raman spectra for starch (see Supplementary Materials) [11,26]. As expected, autoclave-disrupted *C. zofingiensis* accumulated small starch granules (~3 µm), likely overestimated in size due to heat-induced swelling (see Figures S2a and S2b).

To understand the relation between cellular phenotype and glucose concentration in the culture medium, we measured cell size distributions using a commercial impedance flow cytometer on day 7 after cell seeding. Figure 2b shows the size distributions of the cells incubated in low- and high-glucose media. In the low-glucose condition, the cell size was smaller (~7.2 µm) while its concentration reached a higher value of  $(1.26 \pm 0.01) \times 10^7$  cells/mL. On the other hand, the cells incubated in the high-glucose medium had a

concentration of  $(6.213 \pm 0.007) \times 10^6$  cells/mL (~50% lower than the low-glucose case) with significantly larger sizes (~9.4  $\mu\text{m}$ ) and broader size distribution. In addition, cells grown in the low-glucose medium showed a green coloration as opposed to cells grown in the high-glucose medium, which showed a yellowish-orange coloration (Figure 2c). This suggests that in the low-glucose medium, the cells quickly used all the glucose and subsequently resorted to autotrophy, whereas the cells growing in the high-glucose medium showed higher starch and carotenoid accumulation, as seen in the report by Chen *et al.* [27]. After long culture (>60 days), cells showed an orange-red coloration due to carotenoid accumulation likely caused by nitrogen starvation [28], with the carotenoids accumulating to a level detectable using Raman flow cytometry (see Figure S3).

For culture optimization, *C. zofingiensis* cells grown under different conditions were analyzed using our Raman flow cytometer, each measurement taking only a few minutes. Figure 2d shows the violin plots and box plots for cells grown in low-glucose (0.4 g/L) and high-glucose (20 g/L) media for 4, 5, 6, and 7 days (prepared in culture flasks), and cells grown at different glucose concentrations (0.4, 10, 20, 30, 40, and 50 g/L) for 6 days (prepared in 6-well plates). For cells grown in low-glucose medium, starch concentration was maximized on day 4 and decreased from day 5 onwards, in line with observations in the report by Zhu *et al.* in nitrogen-depleted medium [29]. For the high-glucose medium (20 g/L), starch concentration increased steadily until day 6, with a slight decrease on day 7. These data suggest that the cells used glucose in the media to accumulate starch. Once the media glucose was depleted, they used starch for biomass growth. This is common in microalgae, with previous reports indicating that microalgae tend to increase energy storage before mitosis [30]. In addition, Chen *et al.* reported that *C. zofingiensis* cells tend to utilize lipids rather than starch for cell division when glucose was present [27]. Our observations further indicate that the depletion of the media glucose eventually led to the utilization of the cell starch storage. The data in Figure 2b constitutes further evidence that starch accumulation was enhanced in preference to cell proliferation. Starch-rich cells grown at 20 g/L glucose concentration after 7 days showed significantly lower cell concentration and considerably larger sizes than cells grown at low glucose concentration. Regarding glucose concentration dependence, the results show that the cells can accumulate starch effectively under high glucose concentration (up to 20 g/L). However, higher glucose concentrations inhibited high starch accumulation [31,32]. Namely, cells grown at 40 or 50 g/L of glucose reached lower cell concentrations than

cells grown at 20 g/L (data not shown), indicating that high glucose concentrations inhibited biomass production [33].

In addition, we observed that cells accumulated starch more effectively when growing in a flask than when growing in wells. Comparing cells grown at 20 g/L glucose concentration for 6 days from the blue violin plots (grown in flasks) and the green violin plots (grown in 6-well plates) in Figure 2d, the distributions of starch concentration showed similar maximum-starch outliers, but cells grown in flasks showed a higher median than cells grown in 6-well plates. One possible explanation is a difference in surface-to-volume ratio and thus gas exchange, with 6-well plates showing 22% less surface-to-volume ratio than T-25 flasks in the experimental seeding conditions. In conclusion, for the tested temperature, medium, light, and cell-seeding conditions and without cell agitation, the best culture conditions to maximize starch accumulation was found to be 6-day incubation with 20 g/L glucose in a flask to maximize gas exchange surface area.

Obtaining single-cell data makes cell population analysis possible. The box plots and violin plots in Figure 2d show positively skewed distributions. In addition, samples with higher starch content showed wider distributions. Plotting the median and interquartile ranges for each condition (Figure S4) indicates that single-cell starch content exhibited increasing interquartile ranges for increasing median values. We discussed the positively skewed Raman flow cytometry data in the report by Hiramatsu *et al.* [21] as a combination of the common lognormal distribution in single-cell biology and a normal distribution from random noise from the experimental acquisition [21]. An increase in the distribution width as the median increases is characteristic of lognormal distributions, common in intracellular reaction dynamics [34]. This insight would have been impossible using enzymatic quantification, as it obtains the average starch contents for each sample without single-cell resolution.

### **3.2 Comparison with standard methods**

To validate the obtained Raman flow cytometry results, aliquots from these samples were fixed for starch quantification using Lugol staining. Lugol stain develops a dark coloration when binding to starch and can quantify cell starch contents in a limited range of concentrations [12]. Figure 2e shows starch accumulation for 4-day-incubation in the low glucose media that decreases on day 5 and onward, showing agreement with the Raman flow cytometry observations. For high-glucose media, however, all samples show similar coloration, indicating that the starch concentration of the samples is out of range for the Lugol staining

sensitivity. Similarly, Figure 2f shows a clear difference between cells grown at 0.4 g/L glucose and cells grown at higher concentrations but loses contrast among the higher starch accumulations. Image analysis of the Lugol staining brightfield images showed overall agreement with the Raman flow cytometry data and confirmed that high starch concentrations were out of range for Lugol quantification (see Figures S4a and S4b). The Raman flow cytometry results show overall agreement with the Lugol staining results, with sensitivity to a wider range of starch concentrations than Lugol staining.

FT-CARS spectroscopy shows an approximately linear response to the analyte concentration [35]. Consequently, Raman flow cytometry is expected to show an approximately linear response on the single-cell starch concentration, assuming that the starch distribution throughout the cell is fairly homogenous, such that the fraction of cell content measured by Raman flow cytometry is representative of the whole. To show this, cells were seeded under different conditions and Raman flow cytometry was performed. Aliquots of these samples were fixed, counted, and dried for biomass quantification, mechanical cell disruption, and starch enzymatic quantification. It is worth noting that not all samples had enough biomass for mechanical disruption, and only those samples with enough biomass were carried forward. The results of the bulk enzymatic quantification compared to the single-cell Raman flow cytometry screening results are shown in Figures 3a and 3b. The mean starch intensity recorded with Raman flow cytometry was plotted against the mean starch cell content (Figure 3a) and the starch percentage (Figure 3b), and fitted to a linear equation. The distributions for the data in Figure 3 are shown in Figure S5. The Raman flow cytometry signal was acquired across a line in the middle of each cell and only cell-containing spectra were considered for the average. As such, the measured starch is proportional to the mean starch concentration in the cell, while the total starch per cell is affected by the average cell size for each sample. In this dataset, the cells showed size changes for different conditions (see Figure 2b). These results show a similar correlation present for both measurables. Figure S5 shows that the median showed a better correlation to the enzymatic quantification results, as it is more robust against the effect of outliers. The results confirm that Raman flow cytometry could be used for the quantification of mean sample starch when using enzymatic quantification in combination with biomass determination as a gold standard, with the advantage that Raman flow cytometry only required ~2000 events per sample compared to millions of cells for bulk enzymatic quantification, and allowed live cells measurement. It is important to note that FT-CARS intensity values vary between experimental days due to variations in the optical system alignment. Therefore, to use the calibration curve

for data from different days, correcting day-to-day intensity variations is required. For this reason, the calibration curve for Figure 3 cannot be immediately used to calculate the starch content in the data for Figure 2. An additional limitation of the system is that the spectra are acquired along a cylinder across the center of the cell as it flows through the laser spot. We estimate that for a 6- $\mu\text{m}$  cell, our probed volume corresponds to approximately 10% of the cell volume. As starch is usually not distributed homogeneously inside the cell, this is an additional source of cell-to-cell variability. As future work, scanning the laser in the perpendicular direction to the cell flow would increase the volume of the cell being measured by Raman and improve the measurement accuracy.

### 3.3 Cell viability

One of the advantages of Raman flow cytometry is its ability to probe the chemical contents of live cells in a label-free manner, removing the need for time-consuming staining protocols and allowing screening metabolites that lack a specific staining. The current system could be integrated with cell sorting, which would allow the screening and sorting of starch super-accumulating cells. For this approach to be feasible, measured cells need to remain viable following Raman flow cytometry. To test this, chlorophyll-rich *C. zofingiensis* cells and starch-rich *C. zofingiensis* cells were collected following Raman flow cytometry measurement at different laser powers. Three controls with 0 mW laser power were prepared to isolate the cytotoxicity of microfluidic transit and the acoustic focusing: a control (C) seeded under sterile conditions; a flow control (F), passed through the microfluidic system at the standard flow speed for Raman flow cytometry without acoustic focusing; and an acoustic focusing control (AC), passed through the system similarly to F control but with acoustic focusing. The remaining samples were flown through the system with acoustic focusing and exposed to the Ti:Sapphire pulsed laser at the indicated laser powers measured before the focusing objective (see Figure 4). The results confirmed that the microfluidic environment did not affect the cell viability for either chlorophyll-rich or starch-rich cells. Starch-rich cells remained viable (>90%) for all laser powers probed. Chlorophyll-rich cells however showed acute laser-induced cell death, with a drop of viability to ~50% at ~75 mW and viability values below 25% for 200 mW laser power. This is due to the intense two-photon fluorescence excitation of chlorophyll A at the Ti:Sapphire laser wavelength of  $780 \pm 40$  nm that triggers the photodegradation of chlorophyll, causing cell death. Although the current Raman flow cytometer could detect starch with laser powers as low as 100 mW (see Figures S1a and S1b),

the best signal-to-noise ratio was achieved for higher laser powers. This shows that the current system is well suited for sorting low-chlorophyll cells, ideally grown under heterotrophic conditions, but requires further optimization for the non-destructive screening of chlorophyll-rich cells.

#### **4. CONCLUSIONS**

In this report, we showed that Raman flow cytometry has the sensitivity to detect starch and carotenoids of rapidly flowing *C. zofingiensis* microalgal cells (4.89 cm/s) in growth medium at a relatively high event rate (30-100 eps). The single-cell starch content was studied on cells grown in low- and high-glucose mAc media. The cells showed low starch concentrations when grown in mAc medium after 4 days, which decreased at 5, 6, and 7 days. Contrarily, cells showed high starch accumulation when grown in medium supplemented with 20 g/L glucose, which peaked at day 6. These results agree with previous observations that starch is not used during cell division in the presence of glucose and further indicated that glucose depletion led to an increase in cell proliferation and subsequent use of cell starch storage. In addition, high glucose medium also slowed down cell growth while increasing cell size, indicating that starch storage was enhanced while proliferation was reduced. When using even higher glucose concentrations (>30 g/L), both growth and starch accumulation were inhibited. Lugol staining and imaging confirmed these results, but lacked the sensitivity of the Raman flow cytometry measurements. The mean single-cell starch mass ratio and starch percentage obtained from enzymatic starch quantification showed a linear dependence on Raman flow cytometry starch peak intensity, validating that this technique can be used to quantify the mean sample starch. Viability measurements confirmed the suitability of this method to measure and collect starch-rich live cells but showed high laser phototoxicity for chlorophyll-rich cells. These results indicate that Raman flow cytometry is a promising technique for high-throughput starch quantification in live single-cells, currently impossible with any other available technique. Our recent report showed that this system can be integrated with a sorting module for starch-rich cell sorting [36]. Future applications will focus on the screening and sorting of starch hyper-producing microalgae following mutagenesis.

#### **5. ACKNOWLEDGEMENTS**

This work was supported by White Rock Foundation, JST PRESTO (JPMJPR1878), JSPS Core-to-Core Program, JSPS Grant-in-Aid for Young Scientists (20K15227), Grant-in-Aid for JSPS Fellows (19F19805), Nakatani Foundation, Ogasawara Foundation, and Kurita Foundation.

### **Author information**

#### **Corresponding Author**

Kotaro Hiramatsu – **ORCID iD:** <https://orcid.org/0000-0003-0767-019X> ; **E-mail:** kotaro@g.ecc.u-tokyo.ac.jp

#### **Authors**

Julia Gala de Pablo – ORCID iD: <https://orcid.org/0000-0003-0557-9632>

Matthew Lindley – ORCID iD: <https://orcid.org/0000-0002-8164-8479>

Akihiro Isozaki – ORCID iD: <https://orcid.org/0000-0003-0391-9832>

Keisuke Goda – ORCID iD: <https://orcid.org/0000-0001-6302-6038>

#### **Author Contributions**

JGP, ML, KH developed the Raman flow cytometry setup. JGP, KH, and KG conceptualized starch screening of microalgae. JGP performed all the experiments and data analysis. KG supervised the work. The manuscript was written through the contributions of all authors. All authors have approved the final version of the manuscript.

#### **Notes**

KG is a shareholder of CYBO and LucasLand. The other authors declare no competing financial interest.

## **6. REFERENCES**

- [1] F. Di Caprio, A. Visca, P. Altimari, L. Toro, B. Masciocchi, G. Iaquaniello, F. Pagnanelli, Two stage process of microalgae cultivation for starch and carotenoid production, *Chemical Engineering Transactions*. 49 (2016) 415–420. <https://doi.org/10/gjf8ss>.
- [2] R. Madadi, H. Maljaee, L.S. Serafim, S.P.M. Ventura, Microalgae as Contributors to Produce Biopolymers, *Mar Drugs*. 19 (2021) 466. <https://doi.org/10.3390/md19080466>.
- [3] I. Gifuni, G. Olivieri, I.R. Krauss, G. D’Errico, A. Pollio, A. Marzocchella, Microalgae as new sources of starch: Isolation and characterization of microalgal starch granules, *Chemical Engineering Transactions*. 57 (2017) 1423–1428. <https://doi.org/10/gjf8th>.
- [4] F. Di Caprio, R. Chelucci, I. Francolini, P. Altimari, F. Pagnanelli, Extraction of microalgal starch and pigments by using different cell disruption methods and aqueous two-phase system, *Journal of Chemical Technology & Biotechnology*. 97 (2022) 67–78. <https://doi.org/10.1002/jctb.6910>.

- [5] E. Chiotelli, M. Le Meste, Effect of Small and Large Wheat Starch Granules on Thermomechanical Behavior of Starch, *Cereal Chemistry*. 79 (2002) 286–293. <https://doi.org/10.1094/CCHEM.2002.79.2.286>.
- [6] N. Lindeboom, P.R. Chang, R.T. Tyler, Analytical, Biochemical and Physicochemical Aspects of Starch Granule Size, with Emphasis on Small Granule Starches: A Review, *Starch - Stärke*. 56 (2004) 89–99. <https://doi.org/10/bm24vx>.
- [7] K.W. Chew, J.Y. Yap, P.L. Show, N.H. Suan, J.C. Juan, T.C. Ling, D.-J. Lee, J.-S. Chang, Microalgae biorefinery: High value products perspectives, *Bioresource Technology*. 229 (2017) 53–62. <https://doi.org/10.1016/j.biortech.2017.01.006>.
- [8] B. Fernandes, G. Dragone, A.P. Abreu, P. Geada, J. Teixeira, A. Vicente, Starch determination in *Chlorella vulgaris*—a comparison between acid and enzymatic methods, *J Appl Phycol*. 24 (2012) 1203–1208. <https://doi.org/10/czfk4r>.
- [9] A.M. Smith, S.C. Zeeman, Quantification of starch in plant tissues, *Nat Protoc*. 1 (2006) 1342–1345. <https://doi.org/10/dd66tk>.
- [10] Z.U. Rehman, A.K. Anal, Enhanced lipid and starch productivity of microalga (*Chlorococcum* sp. TISTR 8583) with nitrogen limitation following effective pretreatments for biofuel production, *Biotechnology Reports*. 21 (2019) e00298. <https://doi.org/10/gjf82v>.
- [11] Y. Ji, Y. He, Y. Cui, T. Wang, Y. Wang, Y. Li, W.E. Huang, J. Xu, Raman spectroscopy provides a rapid, non-invasive method for quantitation of starch in live, unicellular microalgae, *Biotechnology Journal*. 9 (2014) 1512–1518. <https://doi.org/10/f2r9sb>.
- [12] T. Takeshita, K. Takeda, S. Ota, T. Yamazaki, S. Kawano, A Simple Method for Measuring the Starch and Lipid Contents in the Cell of Microalgae, *CYTOLOGIA*. 80 (2015) 475–481. <https://doi.org/10/ggxzrx>.
- [13] S.A. Borman, Nonlinear Raman Spectroscopy, *Analytical Chemistry*. 54 (1982) 1021A-1026A. <https://doi.org/10/gg54md>.
- [14] A.A. Fung, L. Shi, Mammalian cell and tissue imaging using Raman and coherent Raman microscopy, *WIREs Systems Biology and Medicine*. 12 (2020) e1501. <https://doi.org/10.1002/wsbm.1501>.
- [15] C. Krafft, M. Schmitt, I.W. Schie, D. Cialla-May, C. Matthäus, T. Bocklitz, J. Popp, Label-Free Molecular Imaging of Biological Cells and Tissues by Linear and Nonlinear Raman Spectroscopic Approaches, *Angewandte Chemie International Edition*. 56 (2017) 4392–4430. <https://doi.org/10/f3s7f5>.
- [16] G.T. Taylor, E.A. Suter, Z.Q. Li, S. Chow, D. Stinton, T. Zaliznyak, S.R. Beaupré, Single-Cell Growth Rates in Photoautotrophic Populations Measured by Stable Isotope Probing and Resonance Raman Microspectrometry, *Frontiers in Microbiology*. 8 (2017). <https://doi.org/10.3389/fmicb.2017.01449>.
- [17] Y. He, P. Zhang, S. Huang, T. Wang, Y. Ji, J. Xu, Label-free, simultaneous quantification of starch, protein and triacylglycerol in single microalgal cells, *Biotechnol Biofuels*. 10 (2017) 275. <https://doi.org/10/gjf8tw>.
- [18] M. Herbig, A. Isozaki, D. Di Carlo, J. Guck, N. Nitta, R. Damoiseaux, S. Kamikawaji, E. Suyama, H. Shintaku, A.R. Wu, I. Nikaido, K. Goda, Best practices for reporting throughput in biomedical research, *Nat Methods*. (2022) 1–2. <https://doi.org/10.1038/s41592-022-01483-6>.
- [19] J. Gala de Pablo, M. Lindley, K. Hiramatsu, K. Goda, High-Throughput Raman Flow Cytometry and Beyond, *Acc. Chem. Res.* (2021). <https://doi.org/10.1021/acs.accounts.1c00001>.
- [20] K. Hiramatsu, T. Ideguchi, Y. Yonamine, S. Lee, Y. Luo, K. Hashimoto, T. Ito, M. Hase, J.-W. Park, Y. Kasai, S. Sakuma, T. Hayakawa, F. Arai, Y. Hoshino, K. Goda, High-throughput label-free molecular fingerprinting flow cytometry, *Science Advances*. 5 (2019) eaau0241. <https://doi.org/10/ggtkm4>.
- [21] K. Hiramatsu, K. Yamada, M. Lindley, K. Suzuki, K. Goda, Large-scale label-free single-cell analysis of paramylon in *Euglena gracilis* by high-throughput broadband Raman flow cytometry, *Biomedical Optics Express*. 11 (2020) 1752. <https://doi.org/10/gg4bx5>.
- [22] S. Sakuma, Y. Kasai, T. Hayakawa, F. Arai, On-chip cell sorting by high-speed local-flow control using dual membrane pumps, *Lab Chip*. 17 (2017) 2760–2767. <https://doi.org/10/gjf8zt>.
- [23] M. Lindley, J. Gala de Pablo, R. Kinegawa, K. Hiramatsu, K. Hiramatsu, K. Hiramatsu, K. Goda, K. Goda, Highly sensitive Fourier-transform coherent anti-Stokes Raman scattering spectroscopy via genetic algorithm pulse shaping, *Opt. Lett.*, OL. 46 (2021) 4320–4323. <https://doi.org/10.1364/OL.434054>.

- [24] K. Fučíková, L.A. Lewis, Intersection of *Chlorella*, *Muriella* and *Bracteacoccus*: Resurrecting the genus *Chromochloris* Kol et Chodat (Chlorophyceae, Chlorophyta), *Fottea*. 12 (2012) 83–93. <https://doi.org/10/gjf8s7>.
- [25] D. Cheng, D. Li, Y. Yuan, L. Zhou, X. Li, T. Wu, L. Wang, Q. Zhao, W. Wei, Y. Sun, Improving carbohydrate and starch accumulation in *Chlorella* sp. AE10 by a novel two-stage process with cell dilution, *Biotechnology for Biofuels*. 10 (2017) 1–14. <https://doi.org/10/gjf8r6>.
- [26] Y. Liu, Y. Xu, Y. Yan, D. Hu, L. Yang, R. Shen, Application of Raman spectroscopy in structure analysis and crystallinity calculation of corn starch, *Starch - Stärke*. 67 (2015) 612–619. <https://doi.org/10/f27hvr>.
- [27] T. Chen, J. Liu, B. Guo, X. Ma, P. Sun, B. Liu, F. Chen, Light attenuates lipid accumulation while enhancing cell proliferation and starch synthesis in the glucose-fed oleaginous microalga *Chlorella zofingiensis*, *Scientific Reports*. 5 (2015) 1–10. <https://doi.org/10/f7s4rk>.
- [28] M. Rise, E. Cohen, M. Vishkautsan, M. Cojocar, H.E. Gottlieb, S. (Malis) Arad, Accumulation of Secondary Carotenoids in *Chlorella zofingiensis*, *Journal of Plant Physiology*. 144 (1994) 287–292. <https://doi.org/10/fzkgw4>.
- [29] S. Zhu, W. Huang, J. Xu, Z. Wang, J. Xu, Z. Yuan, Metabolic changes of starch and lipid triggered by nitrogen starvation in the microalga *Chlorella zofingiensis*, *Bioresource Technology*. 152 (2014) 292–298. <https://doi.org/10.1016/j.biortech.2013.10.092>.
- [30] L. de Winter, A.J. Klok, M. Cuaresma Franco, M.J. Barbosa, R.H. Wijffels, The synchronized cell cycle of *Neochloris oleoabundans* and its influence on biomass composition under constant light conditions, *Algal Research*. 2 (2013) 313–320. <https://doi.org/10.1016/j.algal.2013.09.001>.
- [31] T. Chen, J. Liu, B. Guo, X. Ma, P. Sun, B. Liu, F. Chen, Light attenuates lipid accumulation while enhancing cell proliferation and starch synthesis in the glucose-fed oleaginous microalga *Chlorella zofingiensis*, *Sci. Rep.* 5 (2015) 14936.
- [32] P.-F. Ip, F. Chen, Production of astaxanthin by the green microalga *Chlorella zofingiensis* in the dark, *Process Biochemistry*. 40 (2005) 733–738. <https://doi.org/10.1016/j.procbio.2004.01.039>.
- [33] G.H. Gim, J.K. Kim, H.S. Kim, M.N. Kathiravan, H. Yang, S.-H. Jeong, S.W. Kim, Comparison of biomass production and total lipid content of freshwater green microalgae cultivated under various culture conditions, *Bioprocess Biosyst Eng.* 37 (2014) 99–106. <https://doi.org/10.1007/s00449-013-0920-8>.
- [34] C. Furusawa, T. Suzuki, A. Kashiwagi, T. Yomo, K. Kaneko, Ubiquity of log-normal distributions in intra-cellular reaction dynamics, *Biophysics*. 1 (2005) 25–31. <https://doi.org/10/d39jmt>.
- [35] K. Hiramatsu, Y. Luo, T. Ideguchi, K. Goda, Rapid-scan Fourier-transform coherent anti-Stokes Raman scattering spectroscopy with heterodyne detection, *Opt. Lett., OL*. 42 (2017) 4335–4338. <https://doi.org/10.1364/OL.42.004335>.
- [36] M. Lindley, J. Gala de Pablo, W. Peterson, A. Isozaki, K. Hiramatsu, K. Goda, High-Throughput Raman-Activated Cell Sorting in the Fingerprint Region, *Advanced Materials Technologies*. n/a (2022) 2101567. <https://doi.org/10.1002/admt.202101567>.

## 7. FIGURES

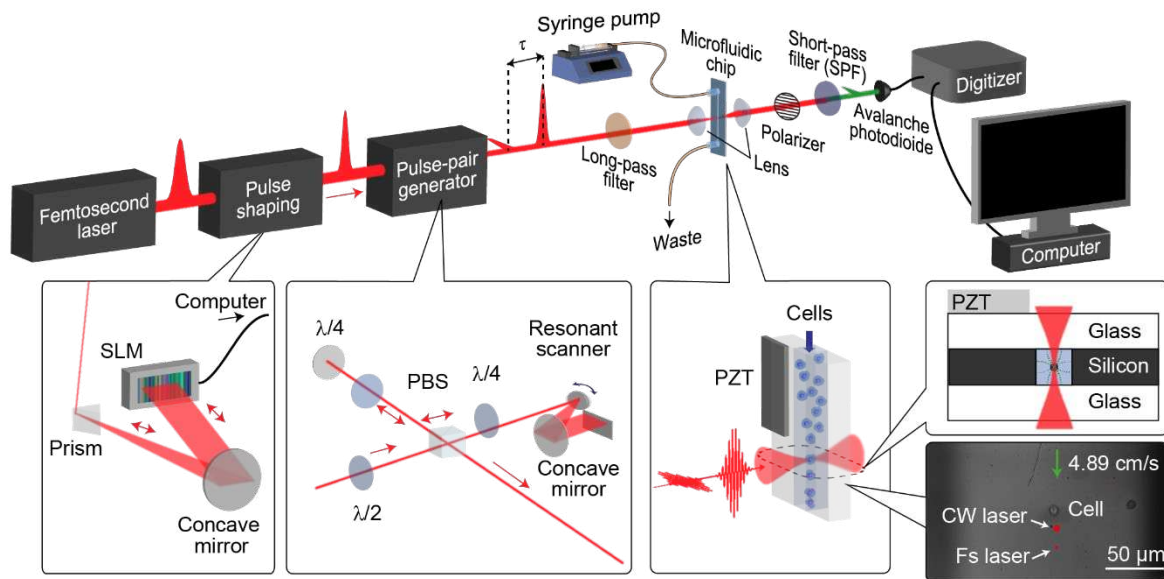


**Figure 1: Schematic of the FT-CARS flow cytometer.** A broadband femtosecond laser is used as the system light source. Dispersion compensation is done in a pulse-shaping module. A Michelson interferometer is used to produce pulse pairs with scanned delay. A long pass filter removes the blue edge of the pulse to improve the detection of the anti-Stokes shifted light. Lenses before and after the sample focus the laser spot. The sample is flown through a microfluidic chip using a syringe pump and acoustic focusing, and crosses the laser beam, obtaining vibrational information of a line across the cell. After the sample, a polarizer removes the pump, and a short pass filter only allows the blue edge of the pulse to reach the avalanche photodetector. The signal is digitized to a computer for further analysis. The bright-field image of a cell during acquisition is shown, where the linear velocity of the cell ( $4.89 \pm 0.09$  cm/s) is indicated. The approximate positions and sizes of the continuous wave (CW) and femtosecond (Fs) laser spots are indicated for illustrative purposes.

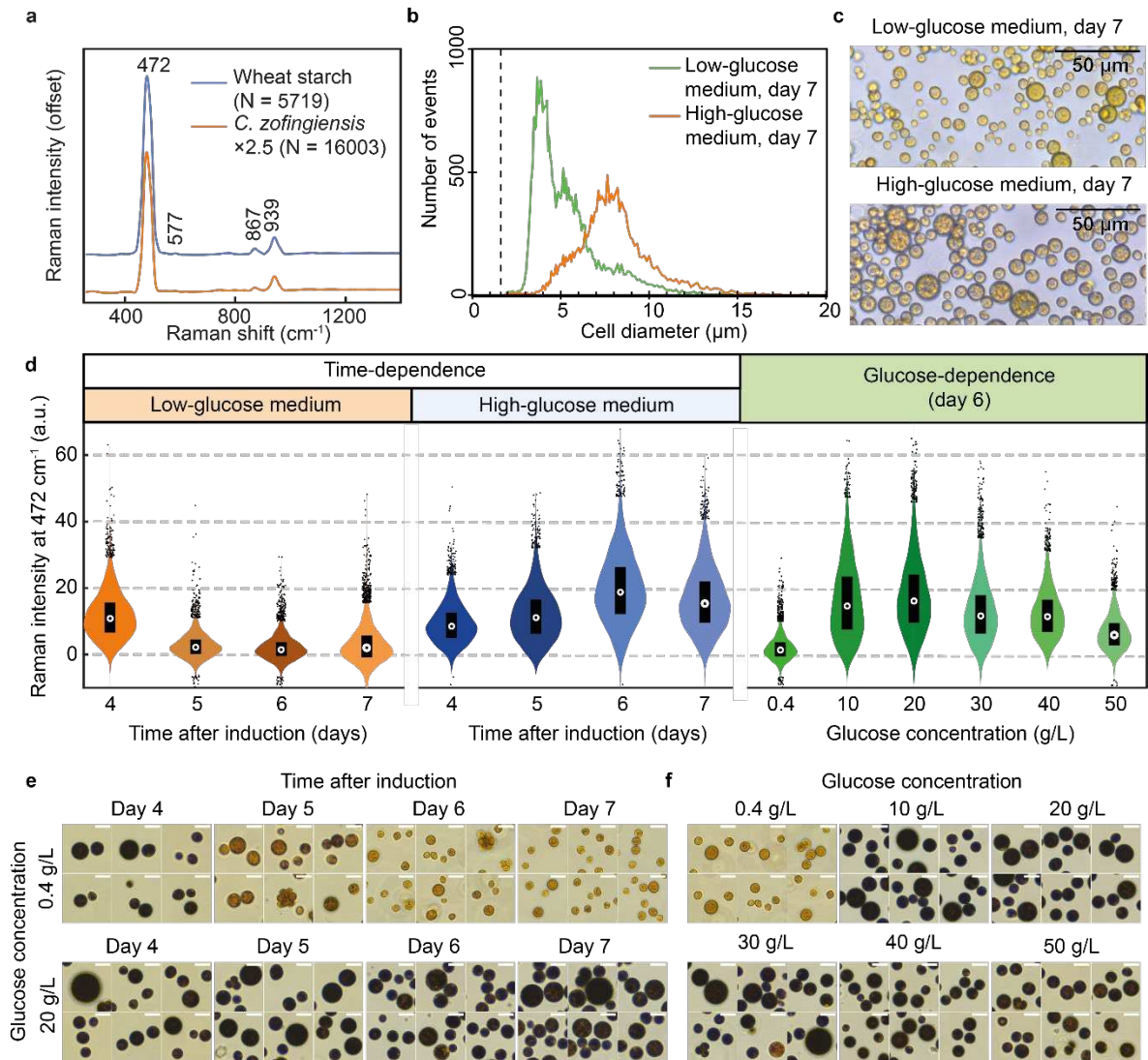


**Figure 2: Optimization and characterization of growth parameters.** a) Average signal of wheat starch and starch-rich *C. zofingiensis* cells incubated with 20 g/L glucose. Note that the *C. zofingiensis* average was multiplied by a factor of 2.5 to increase visibility. The positions of the main Raman bands are indicated. N indicates the number of events used for averaging the Raman intensity. b) Cell diameter measured with impedance flow cytometry for cells grown in low- and high-glucose media after 7 days. The minimum size measurable with this system is indicated with a dashed line. c) Color microscopy images of the cells from b). d) Violin plots for the single-cell intensity of the Raman peak at 472  $\text{cm}^{-1}$  grown in low- and high-glucose media. The glucose dependence data corresponds to 6 days of incubation. e) Color microscopy images of cells from the samples analysed in d) grown in low- (top row) and high-glucose media (bottom row) following Lugol staining. A dark precipitate is formed in the presence of starch. f) Color microscopy images

of the samples analysed in the glucose-dependence experiment in d) following Lugol staining. Scale bars: 10  $\mu\text{m}$ .

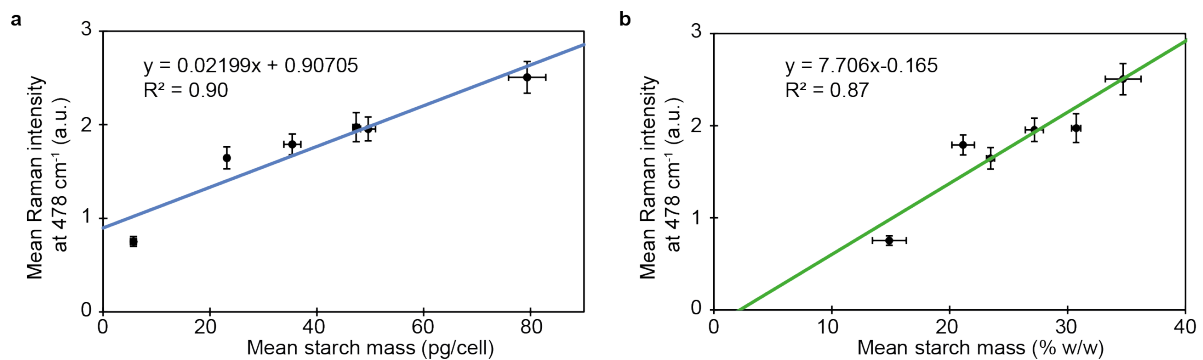


**Figure 3: Starch enzymatic quantification versus Raman flow cytometry.** a) Mean Raman intensity at the 478  $\text{cm}^{-1}$  starch band versus mean starch content per cell from bulk enzymatic quantification. b) Mean Raman intensity at the 478  $\text{cm}^{-1}$  starch band versus mean starch mass percentage content per cell. Error bars correspond to the error propagated from the standard deviation of the UV-Vis absorbance values and the standard error of the mean Raman intensity at 478  $\text{cm}^{-1}$ . Linear fits with equations and  $R^2$  values are shown.

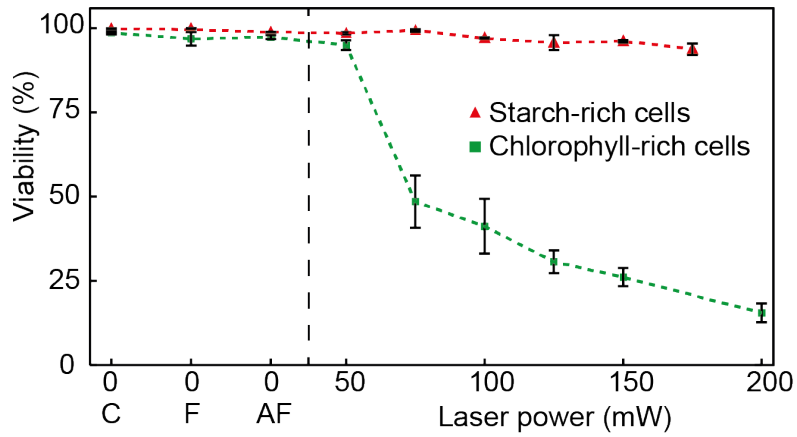


**Figure 4: Cell viability.** Viability of starch-rich cells (orange triangles) and chlorophyll-rich cells (green squares) under increasing laser powers measured under the focusing objective lens. All samples were grown in mAc. The “C” sample (Control) was seeded from the mother culture under sterile conditions. The “F” sample (Flow) was flown through the system without focusing and with 0 mW laser power. The “AF” sample (Acoustic Focusing) was flown through the system with acoustic focusing and 0 mW laser power. The error bars correspond to the standard deviations of three repeats.